GROUND TRUTH OF AFRICAN AND EASTERN MEDITERRANEAN SHALLOW SEISMICITY USING SAR INTERFEROMETRY AND GIBBS SAMPLING INVERSION

Benjamin A. Brooks[1], Neil Frazer[1], Francisco Gomez[2], and Eric A. Sandvol[2]

University of Hawaii[1] and University of Missouri[2]

Sponsored by Air Force Research Laboratory

Contract No. F19628-03-C-0107

ABSTRACT

Comprehensive Nuclear-Test-Ban Treaty (CTBT) verification is dependent on the ability to locate and determine source parameters of small (< M 5.5) and shallow seismic events that have been recorded by sparse seismic networks. Many studies have demonstrated that event calibration significantly improves the location capability of a sparse seismic network; thus, collecting ground truth data for calibration purposes is essential to the operational adequacy of the International Monitoring System (IMS) network.

In our study, we are using InSAR to provide much-needed ground truth (GT) events for a large region currently covered by a very small number of GT5 or better events. Additionally, by applying Gibbs Sampling, a powerful non-linear inversion technique, to the problem of inverting InSAR data for earthquake parameters, we specifically address uncertainties in the GT events and introduce a methodology that should be of use to the entire monitoring community.

In general our work is focusing on shallow earthquakes with moderate magnitudes (M > 5.0). Existing seismic networks and location algorithms can provide adequate epicenter and magnitude estimates but focal depth and mechanism are often poorly constrained. For example, we have measured the co-seismic displacement field for the December 26, 2003 Bam earthquake in central Iran. Using this displacement field we have inverted for the hypocentral location. We plan to invert for the origin time using available seismic phase data. During the past decade, there have been a number of moderate, shallow earthquakes in North Africa and central/east Africa, as well as parts of the eastern Mediterranean region, for which InSAR data may be available to help fill in gaps in calibration seismic events.

In addition to our analysis of specific GT events, we are refining the coupled InSAR/Gibbs Sampling method so that it may be more widely used by the monitoring community. Recent algorithmic advances include: (1) development of a more robust technique for determining sampling temperature, an important Gibbs Sampling control parameter; and (2) development of a parallel processing approach to the entire problem that will decrease computational cost and increase robustness of results.

OBJECTIVES

Our research focuses on delivering 5-km ground truth (GT5) or better locations for seismic events in North and East Africa and the Eastern Mediterranean region using Synthetic Aperture Radar Interferometry (InSAR) geodesy. InSAR, combined with elastic dislocation modeling, is an emerging tool for acquiring GT information in remote areas (Begnaud et al., 2000; Lohmann et al., 2002). Our work will provide much-needed GT events for a large region currently covered by a very small number of GT5 events. Additionally, by applying Gibbs Sampling (GS), a powerful non-linear inversion method, to the problem of inverting InSAR data for earthquake characteristics, the posterior probability distributions for our estimated source parameters will reflect accurate treatment of data variance. This will allow GT event parameters to be compared quantitatively with one another and to be used, for instance, as prior distributions for kriging-based interpolation efforts (Schultz et al., 1998). The general methodology is one that will be of use to the entire monitoring community engaged in regional calibration.

RESEARCH ACCOMPLISHED

At this stage, we divide our accomplished research into two main arenas: (1) algorithm development for earthquake source parameters from InSAR data inversion and (2) delivery of GT events for North and East Africa and the Eastern Mediterranean regions. Below, we describe the general algorithm and illustrate its use for GT-based calibration efforts with an example from the Bam (Iran), 26 December 2003 earthquake.

Algorithm Development

Ground displacements from InSAR deformation maps can be used to invert for earthquake source parameters in a general class of problems called the coseismic geodetic inverse problem. This is written in the standard form, $Gm = d$ where d is a vector of the measured displacements, m is a vector of the source parameters to be inverted for, and G is a matrix of Green's functions which contain the physics relating the two. For a double-couple earthquake source, elastic dislocation Green's functions (Okada,1985) are usually employed and m has 9 components describing the location, orientation and amount of slip for the dislocation. When auxiliary data exist, such as surface traces of coseismic ground rupture or dense seismologic networks, some of these parameters may be eliminated and the general problem can be formulated with fewer free parameters or even linearized allowing for the details of the earthquake slip distribution process to be investigated (Price and Burgmann, 2002).

For the smaller, more remote events that are the focus of this work, however, the full 9-parameter problem must be solved and so the method used to address this multidimensional, non-linear inverse problem becomes important. For instance, gradient-based methods are susceptible to getting stuck in local minima and so more advanced methods are necessary (Murray et al., 1996). Monte Carlo methods (Mosegaard and Sambridge, 2002) such as Gibbs sampling (GS) are particularly powerful tools for multidimensional non-linear inversion and this is the primary routine we will employ for our analysis of the North African seismic events. Although GS has been used in other geophysical problems (Basu and Frazer, 1990; Jaschke, 1997) it has not been explicitly applied to the coseismic geodetic problem to the best of our knowledge.

The Heat Bath (HB) algorithm (Basu and Frazer, 1990; Chapman and Jaschke, 2001; Creutz, 1980; Rebbi, 1984) is an algorithm for Gibbs sampling (GS): it samples from the Gibbs-Boltzmann probability distribution

$$p_j(m) = \frac{e^{-E_j/T}}{\sum_{j=1}^{N_S} e^{-E_j/T}} \quad , \tag{1}$$

where m, referred to here as the model, is a vector of unknown parameters, E_j is the free energy of the j^{th} of N_S states, and T is temperature. In the HB algorithm sampling begins at a high temperature and each parameter, m_j, is visited in sequence. During a visit to the *jth* parameter, the values for the other parameters are held fixed and the system energy, E_j is calculated for each allowed value of m_j. These energies are used to generate a Gibbs-Boltzmann distribution for parameter j, from which a new state for that parameter is chosen by sampling once. After each parameter in the system has been visited once (a cycle called a 'sweep'), the temperature T is lowered by a

small amount and each parameter is visited again. When the desired sampling temperature is reached, samples are collected for later use, but samples obtained during the cooling process are not used.

Ideally, to sample from an arbitrary $\sigma(m)$ one simply defines E in equation (1) by $E(m) = -\ln \sigma(m)$, then samples at $T = 1$; as the number of sweeps becomes infinite the system's equilibrium distribution becomes the Gibbs-Boltzmann distribution (Geman and Geman, 1984; Rothman, 1986) for T=1. It is this theoretical underpinning which makes the GS technique so attractive for GT-based calibration efforts: when properly implemented, GS-estimated parameter distributions from different GT events can be quantitatively compared with one another. Although other authors have used Monte Carlo-based inversion techniques for estimating earthquake source parameters from InSAR and other geodetic data (Cervelli et al., 2001; Lohmann et al., 2002; Wright et al., 2003), it is not clear how inversion results from independent events may be related to one another using these other techniques.

In practice, before beginning to sample at $T = 1$, GS moves to the sampling temperature via a cooling schedule whose characteristics affect the performance of the associated inversion method (Rothman, 1985). If cooled too rapidly, the system will not be in equilibrium, and sampling will be biased, but cooling too slowly is computationally inefficient. A common practice is to cool very slowly from a high temperature to T^*, the critical temperature at which a phase change occurs (Basu and Frazer, 1990). At T^*, low-E models are preferred, but the system is still warm enough for the sampler to escape from local energy minima. Below T^* the system is at least partly frozen, and successive samples tend to have the same value. If $T^* < 1$, it is straightforward to sample at $T = 1$; however, it is practically impossible to sample at $T = 1$ if $T^* > 1$. Moreover, it follows from equation (1) that sampling at T^* gives samples from $\sigma(m)^{1/T^*}$ which is a much broader distribution than $\sigma(m)$ if $T^* > 1$. As $\sigma(m)$ is multidimensional, correcting for this T-scaling is difficult and so has been neglected in previous GS implementations. In our recent work (Brooks and Frazer, in review), we derive an effective correction for the T-scaling in GS results that allows unbiased sampling from an arbitrary $\sigma(m)$, even if $T^* > 1$.

For a given inverse problem, how likely is it that T^* is greater than unity? The answer is rooted in the relationship between T^* and data variance, ν^2. Consider a thought experiment in which data from an event are measured simultaneously by less precise and more precise equipment. The more precise measurements will yield data with variances ν^2 / k^2 where $k > 1$. If the squared residual, $(d - G(m))^T C^{-1} (d - G(m))$ is used for $E(m)$ in equation (1), then a factor k^2 will enter the numerator of the exponent. The physics of the 'melt' hasn't changed, so when k increases (data variance decreases), T^* will increase. This reveals an interesting irony associated with GS-based inversion: when signal-to-noise ratio (SNR) is higher (i.e., the data variances are smaller and the data are qualitatively 'better') T^* is more likely to be greater than unity, and the uncorrected GS procedure is less likely to be sampling from the true distribution, $\sigma(m)$.

We build upon our recent advances and delineate a general method of inverting InSAR data for earthquake source parameters and GT-based calibration efforts. Important aspects include determination of realistic data variance values for InSAR data and, because of the large number of parameters in the inversion (typically >= 9) and the large number of data points (typically tens of thousands for InSAR data sets), data decimation issues. Additionally, we address the possibilities of increasing performance through parallel processing.

We implement our algorithm as follows:

1) Data preparation.
   a) Form interferograms for the GT event (Begnaud et al., 2000), see below, Figure 1a. Our InSAR processing strategy is standard with a small number of exceptions. We process the SAR data using the Gamma Remote Sensing suite of processing tools. In the Middle East region, we have used these tools to construct high-resolution (20 meter pixel) DEM data for regions in Northern Syria and Lebanon (Gomez et al., in review). To remove the signal of the surface topography, we use either: 1) DTED level-1 data; 2) Shuttle Radar Topographic Mission (SRTM) data; 3) existing DEM data (if resolution is 100 meter/pixel or better); or, 4) we construct a high-resolution DEM data using ERS1/2 tandem data. We employ recently developed methods involving minimum-cost-flow algorithms weighted by interferometric coherence to better unwrap patchy interferograms (Chen and Zebker, 2000; Constantini, 1998).

b) Convert radar line of sight (LOS) phase values to range change values with length units (Figure 1b).
c) Crop the image so that it contains most pertinent earthquake related ground motions (Figure 1c).
d) Mask out the near-field signal and, for the whole scene (including the area that was excluded during cropping) determine the data variance, v^2 , in the far field from the co-seismic deformation (Figure 1c). To the extent that atmospheric conditions are consistent across an image, v^2 is an empirical measure of the likely atmospheric contribution to measured phase in the coseismic interferogram. If multiple interferograms are available, then variance can be determined on a pixel-by-pixel basis; if not, then v^2 will be used for each measurement point in the data set and will represent a conservative estimate of variance.
e) Because typical InSAR data sets may comprise thousands of pixels, computational restrictions require that the data be decimated (Figure 1d). Currently we employ the quadtree method (Jónsson et al., 2002), a decimation technique that divides a data block if differences between maximum and minimum values in the block are greater than some threshold value.

2) Data analysis.
a) On one CPU, run a series of 'Short-Runs' (Basu and Frazer, 1990) to determine a range of sampling temperatures, T_s (Figure 2). The T_s range is determined with a series of fixed-temperature 'short runs' for five starting models. A short run consists of 25 sweeps over the parameter space, far fewer sweeps than for an actual inversion. The energy of the final model from each short run is thus a function of short-run starting model and short-run temperature: $E(m_s,T)$. $E(m_s,T)$, is averaged over the starting model, and the T_s range is taken to be the temperature that minimizes the averaged E, or, if there is no minimum, the temperature at which averaged E begins to increase.
b) On as many CPUs as possible, synchronously run the GS algorithm, with each CPU using a different T_s from the narrowed range determined from the short-runs. Here, it is important to note the slight change in nomenclature from T^* to T_s. Previous GS implementation focused on sampling at only one value, T^* . By sampling over a range of values, however, we evaluate various choices for T_s and iteratively approach an optimal value. Additionally, because the parameter value from the previous sweep is used in the sampling of the current sweep, the GS algorithm is not easily parallelizable in the sense of passing multiple computations from one GS run to multiple CPUs. Thus, the limiting factor for parallelizing the GS routine is the objective function itself, in this case, Okada's solutions for surface displacements due to a dislocation embedded in an elastic half-space. For these routines, the computational cost of message passing is greater than the cost of simply continuing the routine on one processor.
c) Construct a plot of T_s vs. E_s, where E_s is the median E values obtained from all of the samples at T_s (Figure 2b). If the plot shows an obvious minimum, then the posterior distributions corresponding to this minimum is the preferred solution. If there is no minimum, then, most likely, the T_s range determined from the short-runs is too narrow and more GS runs should be performed at a wider range of temperature values.
d) Inspect the posterior distributions from the GS runs, using the $T_s > 1$ correction if necessary (Brooks and Frazer, in review) (Figure 3). Posterior distributions usually will converge towards a solution as the most appropriate T_s is approached.

In our experience with InSAR datasets of ~250 surface measurements the entire process, including non-automated aspects (data masking, etc.) should take ~ 2-3 days with an array of 10 modern computers

GT Example: The Bam earthquake

The M_w 6.5 Bam, Iran, earthquake of 26 December, 2003 did not exhibit major macroscopic ground rupture features, but rather it was associated with small-scale surface fissuring (Talebian et al,2004). Focal mechanisms from 3 independent sources (Harvard CMT, NEIC, and Talebian et al (2003)) agree roughly on epicentral location and that the earthquake occurred on a sub-vertical north-south (or east-west) striking plane.

The event was imaged first with descending, then with ascending orbital passes of the Advanced Synthetic Aperture Radar (ASAR) on the European Space Agency's (ESA) Envisat space vehicle. Using the descending data, we created a differential interferogram by differencing a preseismic interferogram (6/11/03 and 12/03/03 acquisition dates, 480 meter perpendicular baseline) and a coseismic interferogram (12/03/03 and 1/07/04 acquisition dates, 540 meter perpendicular baseline). We removed the topographic phase from these data by subtracting a synthetic interferogram created from SRTM data. The results, shown as a map of fringes representing changes in phase values

along the radar's LOS (Figure 1a), yield an especially complete representation of ground motion due to the earthquake. It is important to keep in mind, however, that this image represents only the LOS component of ground deformation and not full 3-d displacements (Wright et al., 2004).

We followed our data preparation and analysis algorithm described above and present the preliminary results in Figures 1-3. The standard deviation of far-field data (ν) was 14.1 mm (Figure 1c) and after cropping and quadtree decimation (Figure 1c) with a threshold of 15cm we performed the GS analysis on 257 data points (Figure 1d). Short-run analysis (Figure 2a) indicated a candidate region of T_s values between 0 and 500. On 8 CPUs we simultaneously ran the full GS algorithm, cooling for 3500 iterations and sampling for 5000 iterations once the cooling schedule reached the particular T_s value. In total, well over 10 million function evaluations were performed on each CPU. The results of plotting median E value versus T_s shows that a value of T_s = 60 yields the lowest median energies, and so it is the most appropriate value of T_s to use when constructing posterior distributions (Figure 3).

Mean values from the preliminary GS results indicate that the earthquake accommodated ~ 2.75 meters of right-lateral strike-slip and negligible dip-slip on a north-south striking, 60° east-dipping fault with dimensions of ~10 x 10 km and an upper edge at ~2500 meters depth. Standard deviations of location parameters (dx, dy, the upper left corner of the dislocation) are of the order of 400 meters. Because $T_s > 1$ in all of our sampling, our correction (Brooks and Frazer, in review) is necessary to tighten the distributions which are sampled from $\sigma(m)^{1/T_s}$ (Figure 3, see discussion above). Although the corrected distributions (red histograms, Figure 3) significantly tighten the sampled distribution (black histograms, Figure 3) it is likely that the 'peakiness' of the correction is an artifact from insufficient number of samples collected. In our tests on synthetic datasets, upon further sampling, the corrected values will converge towards an intermediate distribution shape.

The values determined from this preliminary GS analysis are similar to, though somewhat different than the recently published study of Talebian et al. (2004). The differences are largely due to the inclusion of a secondary thrust fault to the east of the principal strike-slip fault, warranted by consideration of teleseismic P- and SH- bodywaves and strong motion records (Talebian et al,2004). It is possible that the relatively shallow mean dip (Figure 3) of our preliminary solution reflects an averaging of the displacement fields due to two distinct fault slip patches. This discrepancy reflects the possible complications introduced by source complexity if relatively larger earthquakes are to be used for InSAR based GT efforts. Our future work on this earthquake will include inclusion of the ascending interferogram's data and joint inversion with waveform data.

CONCLUSIONS AND RECOMMENDATIONS

1. The Gibbs sampling technique has associated theoretical properties of convergence that make it very attractive for addressing uncertainly issues which arise in inversion of InSAR coseismic data sets for GT efforts. Here, we have developed and presented a general algorithm for implementing GS in GT studies.

2. We give a preliminary test of the GS algorithm on the 2003 Bam (Iran) earthquake and find that it yields results similar to a recently published study, though source complexity may bias the results somewhat. Further sampling is required to provide properly scaled posterior distributions.

3. The apparent source complexity of the Bam earthquake is a good example of why earthquakes smaller than M_w 6 are likely the best candidates for InSAR-based GT studies.

4. There are many different nonlinear inversion/optimization techniques that have been recently implemented to solve for earthquake source parameters from InSAR data (Brooks and Frazer, in review; Cervelli et al., 2001; Lohmann et al., 2002; Sambridge, 1998a; Sambridge,1998b; Wright et al., 2003). The monitoring community's needs for addressing location uncertainties, however, are typically more, well defined and stringent than the usual criteria for a scientific publication. Thus, to best determine which methods are acceptable for GT studies, we recommend that a thorough comparison (empirical and/or theoretical) between inversion techniques be undertaken.

REFERENCES

Basu, A. and L. N. Frazer (1990) Rapid Determination of the Critical Temperature in Simulated Annealing Inversion, *Science*, *249*, 1409-12

Begnaud, M. L., A. A. Velasco and L. K. Steck (2000) Utilizing results from InSAR to develop seismic location benchmarks and implications for seismic source studies, in *22nd Annual DOD/DOE Seismic Research Symposium*, New Orleans, LA

Brooks, B. and L. N. Frazer (in review) Gibbs sampling from an arbitrary distribution, inversion and a test for multimodality, with an application to the coseismic geodetic problem, *Geophys. J Int.*

Cervelli, P., T. Kato, M. H. Murray, P. Segall and Y. Aoki (2001) Estimating source parameters from deformation data, with an application to the March 1997 earthquake swarm off the Izu Peninsula, Japan, *Journal of Geophysical Research B: Solid Earth*, *106* (6), 11217-37

Chapman, N. R. and L. Jaschke (2001) Freeze Bath Inversion for Estimation of Geoacoustic Parameters, in *Inverse Problems in Underwater Acoustics*, edited by M. I. Taroudakis and G. Makrakis, pp. 15-35, Springer-Verlag, New York

Chen, C. and H. Zebker (2000) Network approaches to two-dimensional phase unwrapping: intractability and two new algorithms, *Journal of the Optical Society of America*, *17*, 401-14

Constantini, M. (1998) A novel phase unwrapping method based on network programming, *IEEE Transactions on Geoscience and Remote Sensing*, *36*, 813-21

Creutz, M. (1980) Monte-Carlo study of quantized SU(2) gauge theory, *Phys. Rev. D*, *21*, 2308

Geman, S. and D. Geman (1984) Stochastic relaxation, Gibbs distributions and the Bayesian restoration of images, *IEEE Trans. Patt. Analysis Mach. Int.*, *6*, 721-41

Gomez, F., M. Khawlie, C. Tabet, K. Khair, A. N. Darkal and M. Barazangi (in review) Neotectonics of the northern Dead Sea fault system in Lebanon and Syria based on SAR imagery and high resolution DEM data, *Earth and Planetary Science Letters*

Jaschke, L. (1997) Geophysical Inversion by the Freeze Bath Method with an Application to Geoacoustic Ocean Bottom parameter Estimation, Ph.D. thesis, University of Victoria

Jónsson, S., H. Zebker, P. Segall and F. Amelung (2002) Fault slip distribution of the 1999 Mw 7.1 Hector Mine, California, earthquake, estimated from satellite radar and GPS measurements, *Bull. Seism. Soc. Am.*, *92* (4), 1377-89

Lohmann, R. B., M. Simons and B. Savage (2002) Location and mechanism of the Little Skull Mountain earthquake as constrained by satellite radar interferometry and seismic waveform modeling, *J. Geophys. Res.*, *107* (6)

Mosegaard, K. and M. Sambridge (2002) Monte Carlo analysis of inverse problems, *Inverse Problems*, *18*, 29-54

Murray, M. H., G. A. Marshall, M. Lisowski and R. S. Stein (1996) The 1992 M=7 Cape Mendocino, California, earthquake: Coseismic deformation at the south end of the Cascadia megathrust, *J. Geophys. Res.*, *101* (8), 17,707-17,25

Okada, Y. (1985) Surface deformation due to shear and tensile faults in a half-space, *Bull. Seism. Soc. Am.*, *75*, 1135-54

Price, E. J. and R. Burgmann (2002) Interactions Between the Landers and Hector Mine, California, Earthquakes from Space Geodesy, Boundary Element Modeling, and Time-dependent Friction, *BSSA*, *92* (4), 1450-69

Rebbi, C. (1984), in *Applications of the Monte Carlo Method*, edited by K. Binder, pp. 277-98, Springer-Verlag, New York

Rothman, D. H. (1985) Nonlinear inversion, statistical mechanics, and residual statics estimation, *Geophysics*, *50*, 2784-96

Rothman, D. H. (1986) Automatic estimation of large residual statics corrections, *Geophysics*, *51*, 332-46

Sambridge, M. (1998) Geophysical inversion with a neighborhood algorithm, 1, Searching a parameter space, *Geophys. J. Int.*, *138*, 479-94

Sambridge, M. (1998) Geophysical inversion with a neighborhood algorithm, 2, Appraising the ensemble, *Geophys. J. Int.*, *138*, 727-46

Schultz, C., S. Myers, J. Hipp and C. Young (1998) Nonstationary Bayesian kriging: application of spatial corrections to improve seismic detection, location and identification, *Bull. Seism. Soc. Am.*, *88*, 1,275-1,88

Talebian, M., E. J. Fielding, G. J. Funning, M. Ghorashi, J. Jackson, H. Nazari, B. Parsons, K. Priestly, P. A. Rosen, R. W. Walker and T. J. Wright (2004) The 2003 Bam (Iran) earthquake - rupture of a blind strike-slip fault, *Geophys. Res. Lett.*

Wright, T. J., Z. Lu and C. Wicks (2003) Source model for the Mw 6.7, 23 October 2002, Nenana Mountain Earthquake (Alaska) from InSAR, *Geophys. Res. Lett.*, *30* (18), 1974

Wright, T. J., B. Parsons and Z. Lu (2004) Toward mapping surface deformation in three dimensions using InSAR, *Geophys. Res. Lett.*, *31*, 1607

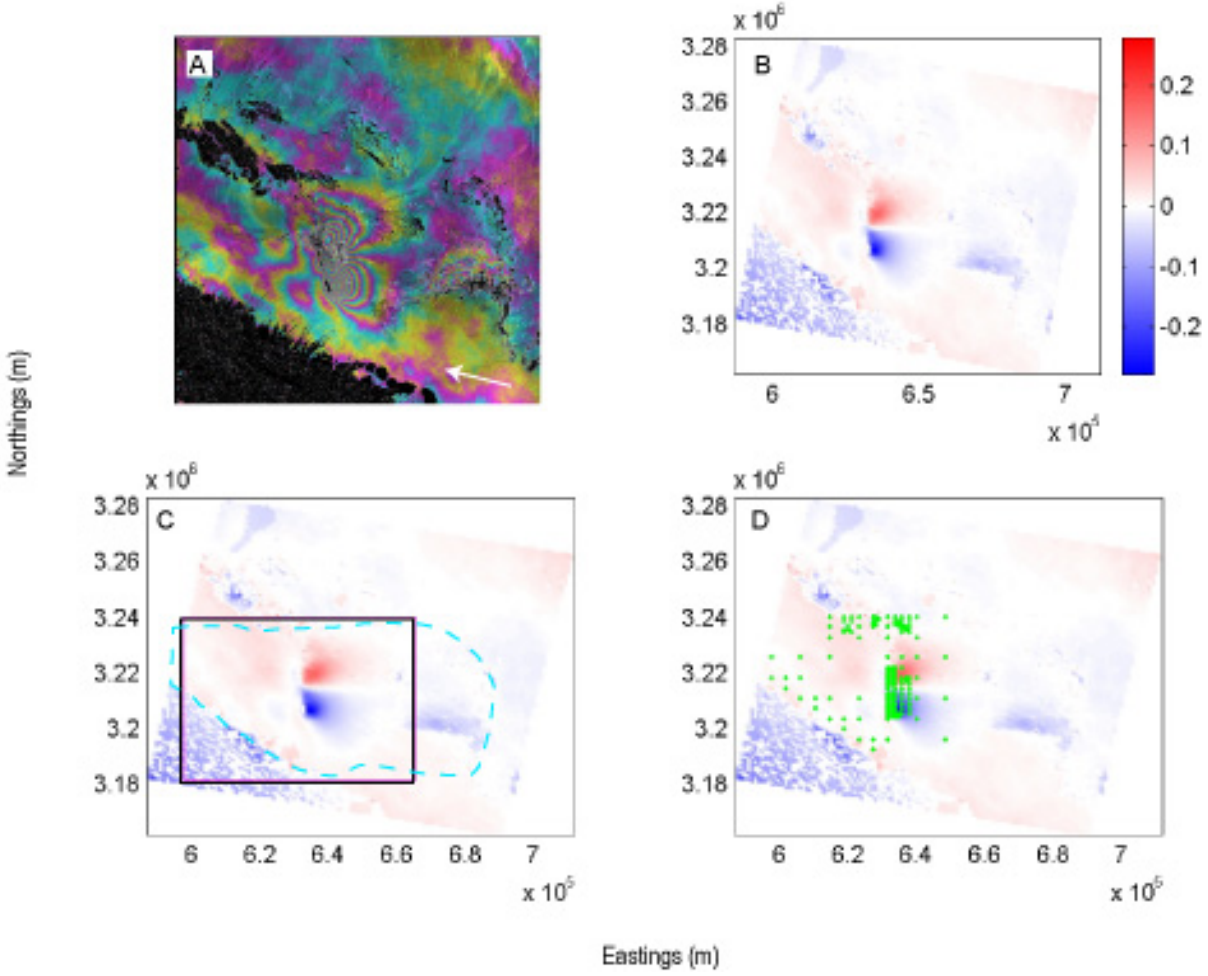

Figure 1. A) Envisat descending differential interferogram showing line of sight (LOS) phase changes (one color cycle represents 28 mm range change) for the Bam 2003 earthquake. White arrow represents look direction of the satellite. B) LOS range change contour map of the data in A, placed in UTM projection. C) Same as B. Black box shows the zone of cropping for GS analysis. Dashed blue line is the mask for calculation of far-field data variance. Only values outside of the mask are included in the calculation. D) Same as C. Green dots show the points retained from quadtree decomposition of the cropped data set.

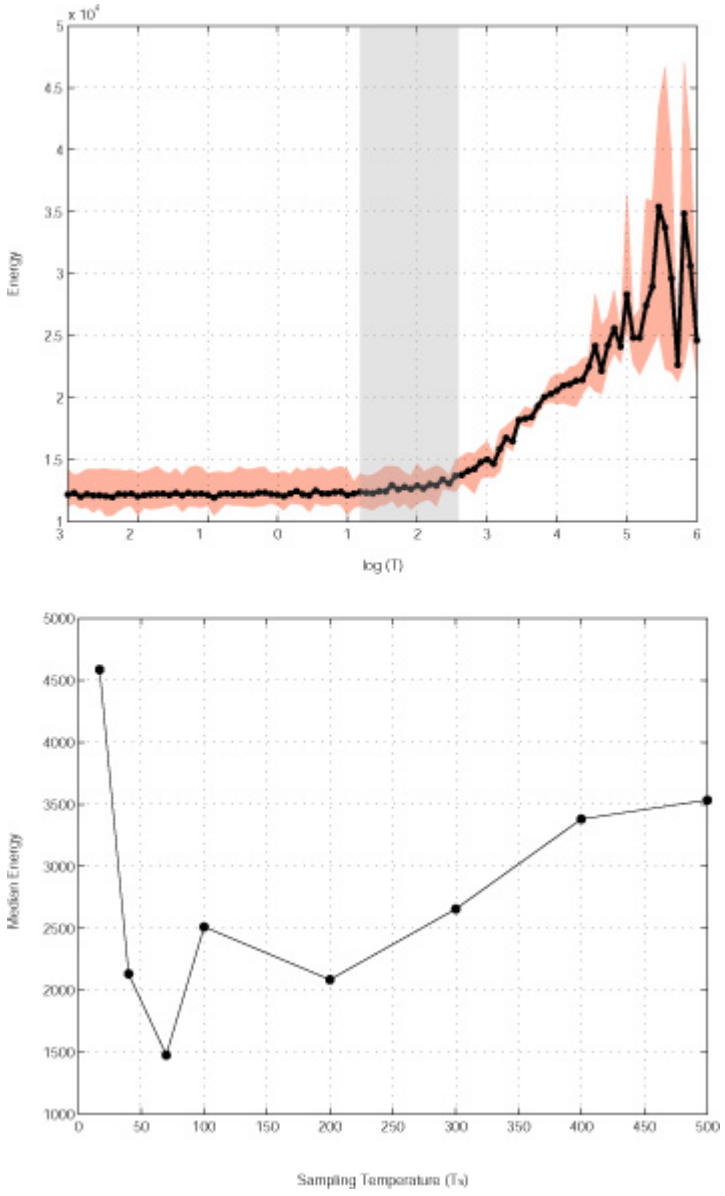

Figure 2. A) Results of Gibbs sampling 'short-run' analysis. The thick black line is the mean energy value of each short run, the pink envelope represents the minimum and maximum energy values of the short run. The grey shaded area indicates the most appropriate range of sampling temperatures. B) Plot of sampling temperature vs. median energy values from full Gibbs sampling runs at a variety of temperatures in the range defined in A. The sampling temperature corresponding to the lowest median energy value is the most appropriate for construction of posterior distributions.

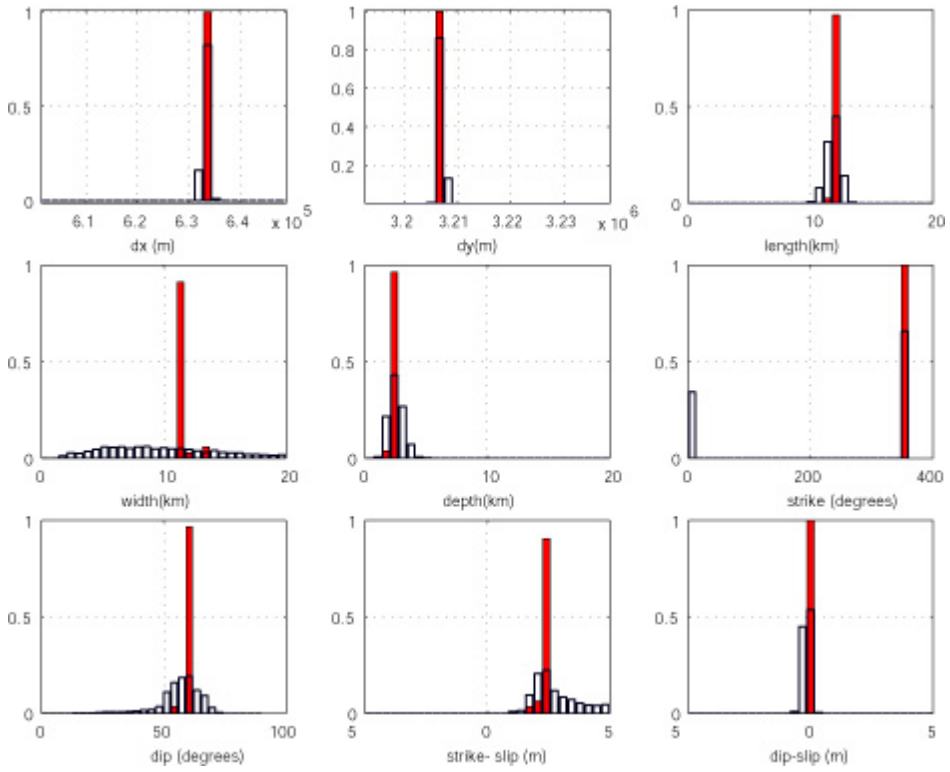

Figure 3. Posterior distributions constructed from full GS run at a sampling temperature of 60. Dx, dislocation east offset; Dy, dislocation north offset; length, dislocation length; width, dislocation width; depth, dislocation upper edge depth; strike, dislocation strike; dip, dislocation dip (using right hand rule with strike); strike-slip, dislocation strike-slip; dip-slip, dislocation dip-slip. The black histograms are from samples collected at T_s. The red histograms represent the correction when sampling occurs at values of $T_s > 1$.